Influence of steel yielding and resin toughness on debonding of wrapped composite joints

He, Pei; Feng, Weikang; Pavlovic, Marko

DOI
10.1016/j.compstruct.2023.116862

Publication date
2023

Document Version
Final published version

Published in
Composite Structures

Composite Structures 312 (2023) 116862

Contents lists available at ScienceDirect

Composite Structures

journal homepage: www.elsevier.com/locate/compstruct

Influence of steel yielding and resin toughness on debonding of wrapped composite joints

Pei He, Weikang Feng, Marko Pavlovic *

Faculty of Civil Engineering and Geosciences, Delft University of Technology, the Netherlands

ARTICLE INFO

Keywords:
CHS
Wrapped composite joints
Steel yielding
Fracture toughness
Debonding
3D DIC

ABSTRACT

The concept of an innovative bonded joining technology where welding is not required is presented as an alternative to traditional welded connection for steel circular hollow section (CHS). Wrapped composite joints have potential to greatly improve fatigue endurance when applied in multi-membered truss structures, e.g. offshore jackets for wind turbines. This paper focuses on characterization of influence of chemical bonding resistance, fracture toughness of resins, and steel yielding on debonding of wrapped composite joints. Uniaxial splice joints (A-joints) are made with GFRP composite material wrapped around steel sections, and tested under static tensile loading conditions until failure. Different chemical bonding properties by application of bonding primer, different types of polymer resins and steel grade are used during the wrapping procedure. Debonding on the bonded interface are identified by surface strain measurements through 3D digital image correlation (DIC) technique. Testing results indicate that steel yielding limits full utilization of the resistance of the bonded interface. Wrapped composite A-joints with high-strength steel exhibits 75% larger ultimate load where yielding is prevented. Larger fracture toughness of toughened vinyl-ester resin contributes to 30% larger displacement of the joints at failure compared to regular vinyl-ester and polyester resins.

1. Introduction

Circular Hollow Sections (CHS) have been extensively used in engineering structures, as shown in Fig. 1, due to its high mechanical/cost efficiency, aesthetic, and good durability [1]. However, when applied in off-shore jacket structure and steel bridges where long-term cyclic loading is prevalent, CHS joints, traditionally formed by welded connecting brace (diagonal) to the chord member, encounter severe fatigue problem [2–4]. The low fatigue endurance of welded CHS joints results from high and complex stress conditions as consequence of local bending of the thin-walled CHS sections and ovalization in the welded intersection areas. Further reasons are stress concentrations attributed to discontinuities at local notches, e.g. at the toes of butt welds and at the toes and roots of fillet welds, where sharp changes of direction occur [5]; and geometric peak stresses due to the non-uniform stiffness distribution at the perimeter of the connection [1]. In addition, welding results in residual stresses in the heat affected zone and embrittlement of the steel material.

Fibre reinforced polymer (FRP) composites, further referred to as composites, have excellent corrosion and fatigue resistance in addition to high strength-to-weight ratio. With tailorable material properties by choosing the type of fibre (glass or carbon, etc.), resin and ease of providing complex shapes through molding and lamination, composites have potential in application with steel hollow sections, as hybrid joints, in fatigue-dominated loading conditions. Increasing interest of research has been seen in last two decades towards strengthening of existing welded circular hollow section (CHS) joints with composite material. The main focus is on steel butt joints [6–7], T joints [8–9], Y joints [10] and gap K joints [11–12]. The conclusion of all previous research is that retrofitting steel CHS joints by composites can enhance loading capacity of those joints substantially, and unfavorable failure modes, i.e., chord ovalization and punching shear, are efficiently mitigated.

Despite improved static behavior of composite-strengthened CHS joints, main load is carried through welded connection, which remains to be a source of stress concentration and brittle failure under fatigue load. To fully unlock application potential of CHS restricted by current welding technology in many cases, the concept of innovative wrapped composite joints is proposed by TU Delft [13] as an alternative to traditional welded joints, as shown in Fig. 2. CHS brace members (diagonals) and the chord member in this case are bonded together by

* Corresponding author.
E-mail address: M.Pavlovic@tudelft.nl (M. Pavlovic).

https://doi.org/10.1016/j.compstruct.2023.116862
Received 6 June 2022; Received in revised form 19 October 2022; Accepted 25 February 2023
Available online 1 March 2023

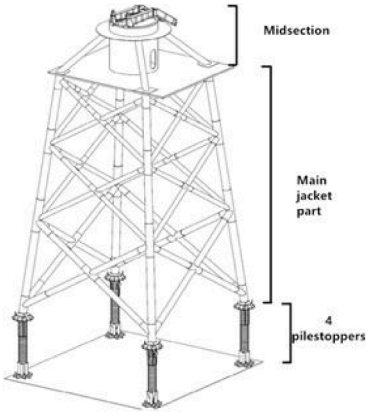

a) Off-shore wind turbine jacket supporting structures

b) Support structures of hydraulic barriers

c) Truss steel bridges

Fig. 1. Engineering application of CHS.

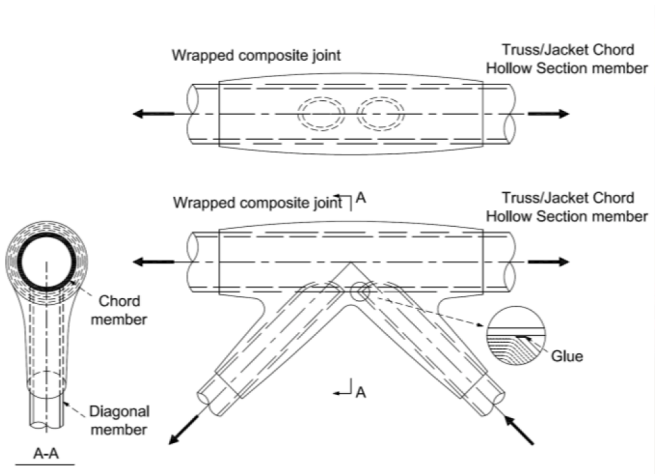

a) General configuration – example K-joint geometry

b) 45° small-scale X joint specimen with Ø 60.3mm braces[18]

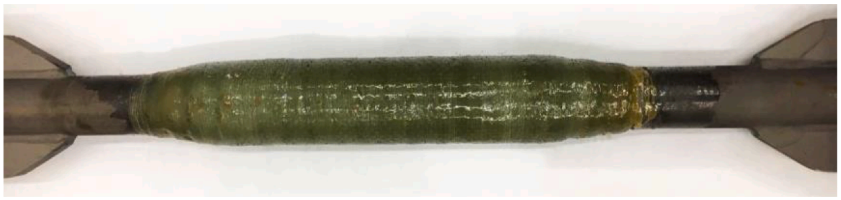

c) Wrapped composite A-joint specimen with Ø 60.3mm steel tube tested and presented in this paper

Fig. 2. Wrapped composite joints.

composite wrap which can be shaped in an optimal manner to decrease stress concentration at the bonded interface. Initial tensile static tests presented in TU Delft [14–16] prove their improved initial stiffness and equivalent load resistance compared to welded joints. The subsequent fatigue experiments validate their lower stiffness degradation and superior fatigue life than the welded joints [17]. Use of high-strength steels (HSS) could lead to large reduction of thickness and therefore weight of the fatigue dominated supporting structures in offshore applications. However, application of HSS is hindered because of very limited fatigue life of the welded joints. Novel wrapped composite joints have potential to overcome this limitation and foster utilization of HSS in structures to reduce weight and CO2 emissions related to steel consumption. Static experiments of wrapped composite joints at different geometric scales are then conducted in different load conditions indicating that full debonding of the bonded interface is the predominant failure mode of the joints [18]. A combined digital image correlation-finite element analysis (DIC-FEA) method is proposed to monitor the debonding crack propagation at the interface of bonded composite-steel joints [19].

Good debonding resistance of the bonded interface is an essential prerequisite for good static behavior of wrapped composite joints, which can be realized by appropriate surface treatment and selection of adhesives. Surface treatments are often required to provide maximum adhesion strength, not only to remove contaminants, but also to increase the difference in surface energy between adhesive and substrate, so good wetting and adsorption of the adhesive is obtained [20]. Surface treatments for steel include but are not limited to solvent degreasing,

Table 1
Test series and specimen designation.

Series number	Test series and specimen naming	Resin type	Bonding treatment	Steel Grade	Connection type	Geometry in Figure number
1	A-Ss-R1-NM_S1/2/3	Resin 1	No Primer	S355	Wrapped composite	3(a)
2	A-Ss-R1-PM_S1/2/3	Resin 1	With Primer	S355	Wrapped composite	3(a)
3	A-Ss-R2-PM_S1/2/3	Resin 2	With Primer	S355	Wrapped composite	3(a)
4	A-Ss-R3-PM_S1/2/3	Resin 3	With Primer	S355	Wrapped composite	3(a)
5	A-Ss-R2-PM_S4/5/6	Resin 2	With Primer	S355	Wrapped composite	3(b)
6	A-Ss-R2-PH_S1/2/3	Resin 2	With Primer	S700	Wrapped composite	3(b)

abrasion and grit blasting [21]. Researchers have found that the best bonded performance of adhesive joints can be achieved by an optimum surface roughness of steel normally determined by grit blasting [22–25].

In the cases to ensure superior durable bonds under particularly adverse environments, the use of bonding primers to pretreat substrates prior to adhesive bonding is becoming of increasing importance in industrial applications [26–27]. It is usually a dilute solution of an adhesive in an organic solvent with the following functions: 1) protect the adherend's surface from oxidation after surface cleaning, extending the time that may elapse between surface preparation and bonding application [28]; 2) improve wetting [29]; 3) serve as a barrier coat to prevent unfavorable reactions between adhesive and adherend [29]; 4) modify the properties of the bonded interface to improve certain characteristics such as peel [30]. Adhesive types also have a significant influence on the bonding quality. The load-bearing capacity is inevitably affected by ductility of adhesives [31–33].

However, current studies are only limited to influence of surface treatment and adhesive types on the behavior of adhesively bonded joints. Further study is needed to characterize their influence on the behavior of novel wrapped composite joints that are directly bonded (laminated) where thin resin layer plays the role of the adhesive. Moreover, the influence of steel grade on the joint resistance should be investigated where high-strength steel has the potential to enhance bonding resistance by preventing yielding of the steel cross section which showed to interact with the debonding process [18].

This paper follows the previous research work in TU Delft [13–19] and aims to quantify and identify the influence of production parameters (i.e., application of bonding primer, polymer resin types and steel grade) on the static resistance of wrapped composite joints. Steel members are connected solely through direct bonding (laminating) the composite wrap in this novel joints as the alternative to welded CHS joints. Six series of A-joint specimens at small-scale (60-mm diameter) are tested in monotonic tensile load until failure. Deformation of the joint during loading is captured by linear variable differential transformers (LVDTs) and surface strain measurements obtained by 3D digital image correlation (DIC) technique.

2. Ultimate load joint experiments

A-joint geometry, namely uniaxial splice joint, is chosen and tested in monotonic tensile load until failure. Selection of this uniaxial and axisymmetric geometry is attributed to ease of production, and the opportunity for clear interpretation of mechanical behavior of the bonding in a simple load condition. A-joint specimens wrapped with and without application of the bonding primer are compared to quantify the influence of difference in chemical bonding properties on the debonding resistance of the joint. Three types of thermoset polymer resins designated as resin 1 and 2 – both vinyl-ester based and resin 3 – polyester based, are used in the wrapping procedure to investigate impact of fracture toughness of resins on the joint resistance. Resin 2 has improved fracture toughness properties compared to resin 1 and resin 3. Mild steel (S355) and high-strength steel (S700) circular hollow sections are used in production of A-joint specimens to quantify the influence of interaction between debonding and steel yielding on the static resistance of the wrapped composite joints.

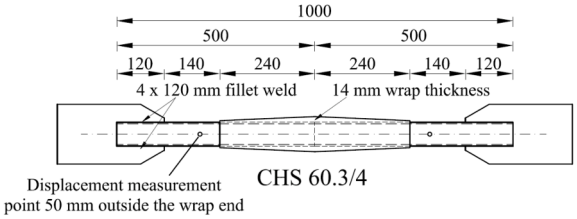

a) Joint type 1: series 1~4 – mild steel (MS)

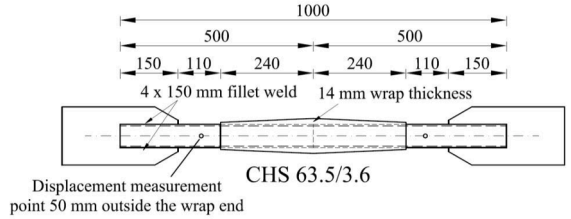

b) Joint type 2: series 5 – mild steel (MS) and series 6 – high strength steel (HSS)

Fig. 3. Geometry of small-scale wrapped composite A-joint specimens for tensile tests (unit: mm).

2.1. Test series

Based on the above-mentioned motivation of the experimental campaign, 6 series of small-scale wrapped composite A-joint specimens are designed for the tensile static experiments, as summarized in Table 1. Configuration of the joint specimen is shown in Fig. 2c) while its geometry with dimensions are shown in Fig. 3a) and Fig. 3b). The main differences of the geometry are in the length of the weld at the end detail and the diameter of the steel tubes. Longer weld is used for series 5 and 6 in which the high strength steel specimens are compared to mild steel specimens. Each series of wrapped composite A-joints tested is accomplished with 3 nominally identical specimens.

Following naming convention is used for series given in Table 1 and used afterwards in analysis of the results: A – Wrapped composite joints, A (uniaxial) geometry; Ss – small-scale; R1, R2, R3 – Resin type used as resin 1, resin 2 and resin 3; PM – with primer / mild steel, NM – no primer / mild steel, PH – with primer / high-strength steel; S1/2/3/etc. - nominally identical specimens, number 1, 2, 3, etc. (S4/5/6 is used in series 5 to distinguish the specimens between series 3 and series 5.).

2.2. Material properties

The CHS profiles (grade S355 and S700) are connected by E-Glass based composite wrap. Bi-directional fibre mats are wrapped (laminated) around steel hollow sections and fibre volume fraction ranging 30–32% is achieved. Note that the composite wrap is directly applied / bonded on the steel tubes without separate adhesive layer so that the failure related to adhesive is eliminated. Grit blasting and chemical degrease is applied on the steel tubes before wrapping to ensure good surface preparation. The alignment of the steel tubes is controlled to be less than 0.5 mm misalignment. The hand lamination (wrapping)

Table 2
Mechanical properties of the composite wrap laminate with resin 2.

Mechanical properties	Average value (and CoV [%])
In-plane compressive strength in x/y direction – $f_{x,c} = f_{y,c}$	200 MPa (3.79)
In-plane compressive modulus in x/y direction – $E_{x,c} = E_{y,c}$	12077 MPa (4.50)
In-plane tensile strength in x/y direction – $f_{x,t} = f_{y,t}$	216 MPa (5.78)
In-plane tensile modulus in x/y direction – $E_{x,t} = E_{y,t}$	11798 MPa (6.37)
In-plane major Poisson's ratio – ν_{xy}	0.15 (6.50)
In-plane shear strength – $f_{xy,v}$	72.2 MPa (2.59)
In-plane shear modulus – G_{xy}	3120 MPa (6.81)

procedure is fulfilled in a couple of stages where the smooth thickness transition and ply drops is achieved as well as good compaction and avoidance of air gaps. No post-curing is applied to the wrapped specimens. Thickness of the composite wrap is maximum at the joint root with the value of 14 mm and decreases to 0 mm at the wrap end, as shown in Fig. 3. The repeatability of the production is assured by using only certified laminators in the factory where the joint are produced. Temperature, humidity, surface roughness and cleans, peroxide type and content, the resin shell and the cleans of the glass fiber and mats are strictly controlled through the quality control and assurance programme.

Mechanical properties of the composite material are determined in case of resin 2 and are summarized in Table 2. The standard tensile/compressive/in-plane shear coupon tests are conducted to obtain these material properties based on ISO standard [34–37].

2.3. Joint experiments set-up

The tensile static experiments of wrapped composite A-joints in series 1–4 are conducted in the MTS 647 Hydraulic Wedge Grip with 600 kN loading capacity equipped with hydraulic clamping heads in Stevin lab 2 of TU Delft, as shown in Fig. 4. The axial load on steel tubes is applied through gripping the endplates welded to the joint. Specimens in series 5–6 are tested in the Universal testing Machine (UTM) with 800 kN loading capacity considering the potential enhancement of the static resistance attributed to use of high-strength steel, see Fig. 5 b) and 5c). Load is applied by displacement control with rate of 1 mm/min to provide quasi-static loading condition.

2.4. Measurement set-up

Two measurement techniques are used in the ultimate load joint experiments. In experiments of series 1 ~ 4), the measurement system

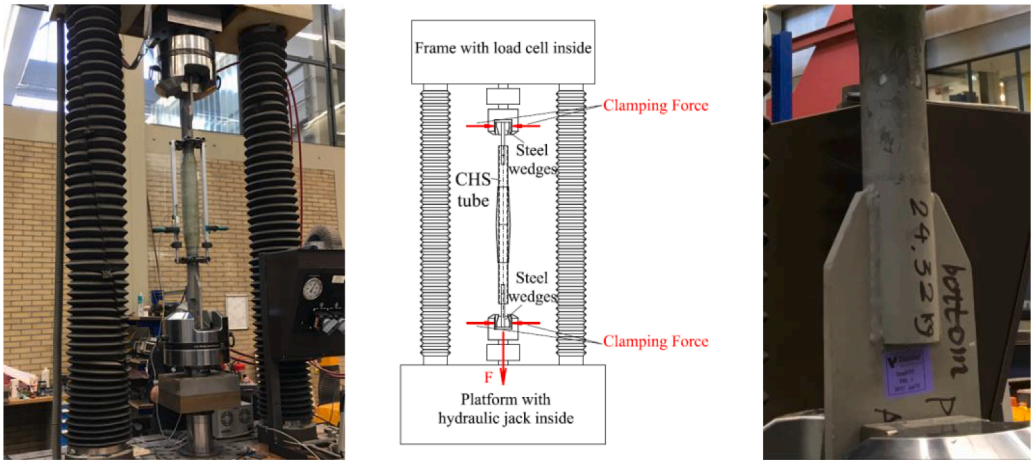

a) Experimental set-up configuration b) Schematic experimental set-up c) Load introduction at the brace end

Fig. 4. Test set-up of small-scale wrapped composite A-joints in series 1–4 under axial tensile load.

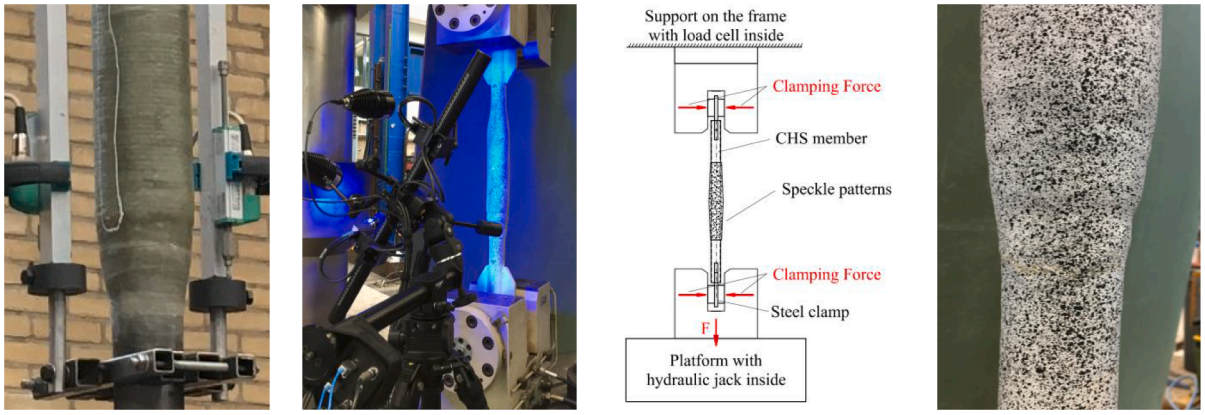

a) LVDTs in series 1-4 b) DIC measurements in series 5-6 c) Schematic experimental set-up d) Spackle pattern

Fig. 5. Measurement technique in series 5–6 using 3D DIC system with live measurement of displacements and strains on the surface of specimens.

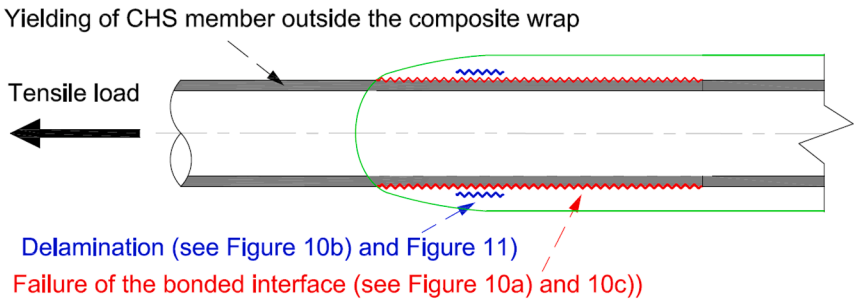

Fig. 6. Failure modes of a wrapped composite A-joint loaded in tension.

based on two Linear Variable Differential Transformers (LVDTs), at front and back is used to capture potential eccentricity and average the data. In the experiments series 5–6, the 3-dimensional (3D) Digital Image Correlation (DIC) system is used to measure both longitudinal extension between ends of the specimens and distribution of surface strain of the joints to indirectly track the propagation of the debonding crack, as shown in Fig. 5. GOM Aramis adjustable base 12MPx system is used which includes two cameras with 12-megapixel resolution, controller and graphical analysis software to acquire and process test data. The $750 \times 610 \times 610$ mm^3 measuring volume is used and speckle patterns are applied on the specimens' surface by spray method with grain size of approximately 2 mm, corresponding to the small-scale joint geometry. Polarized blue light is used to limit influence of variation of ambient light on measurement accuracy.

3. Failure modes of wrapped composite joints

Based on the results of preliminary tensile static tests [14–18] and the results shown in this paper afterwards, the load transfer mechanism and potential failure scenarios of wrapped composites A-joints are identified and schematically shown in Fig. 6. The main load transferring components of the wrapped composite joint are:

- Bonded interface – which connects the CHS members to the composite wrap. The joint load in tension from the steel member is transferred to the composite wrap mainly through mode II (shear) interface behavior.

- Composite wrap – which transfers the joint load from one CHS members to another CHS member. The load transfer is through multi-axial stress state: longitudinal, trough thickness and tangential stresses due to the relatively thick curved laminate.

The failure modes of the wrapped composite A-joints can be divided into four main groups for tensile axial load:

1) Failure of the bonded interface by partial or full debonding. Mode II interface failure is dominant, partially reduced by mode-mixity with Mode I interface stresses at the wrap end due to contraction of the steel cross section after yielding. From the three-point end notched flexure (3ENF) test not presented here, the average value of the mode II critical strain energy release rate is 2 N/mm. The crack initializes at the root of the connection (coincidence of the two CHS members) due to stress concentrations and propagates towards the end of the bonded interface. Thickness profile of the composite wrap is tapered towards the wrap end to reduce the shear stress concentrations and peel stresses at the end of the composite wrap.
2) Failure of the composite wrap by fracture involving micro-scale failure modes of the fibres and resin. Given the quasi-isotropic behavior and relatively large thickness (up to 14 mm) of composite wrap laminate used in the joints, the local failure modes of the composite wrap can be characterized as out-of-plane shear due to delamination and tensile failure (in-plane) of the laminate.
3) Failure of CHS member by yielding next to or inside the composite wrap. Yielding of the steel inside the composite wrap can promote debonding on the bonded interface. Yielding of the steel outside, close to the end of composite wrap can initiate debonding crack from the end of the bonded interface.

Table 3
Test results related to influence of primer and resin.

Series	Specimen	Initial stiffness [kN/mm]	Elastic load limit [kN]	Ultimate load [kN]	Displacement at failure [mm]
1	A-Ss-R1-NM_S1	258.5	196.3	319.9	4.0
	A-Ss-R1-NM_S2	262.5	185.2	314.3	1.8
	A-Ss-R1-NM_S3	261.9	198.3	314.0	2.1
	Average (and COV [%])	261.0 (0.67)	193.3 (2.98)	316.1 (0.86)	2.6 (36.99)
2	A-Ss-R1-PM_S1	255.7	189.1	334.7	3.8
	A-Ss-R1-PM_S2	256.7	195.7	327.0	4.4
	A-Ss-R1-PM_S3	252.2	186.8	324.5	3.4
	Average (and COV [%])	254.9 (0.76)	190.5 (1.98)	328.7 (1.32)	3.9 (10.63)
3	A-Ss-R2-PM_S1	251.8	221.5	335.4	5.1
	A-Ss-R2-PM_S2	241.9	221.4	341.2	4.9
	A-Ss-R2-PM_S3	247.8	234.2	334.7	4.8
	Average (and COV [%])	247.2 (1.65)	225.7 (2.66)	337.1 (0.86)	4.9 (2.53)
4	A-Ss-R3-PM_S1	265.8	179	334.4	3.9
	A-Ss-R3-PM_S2	264.8	186.2	324.3	3.7
	A-Ss-R3-PM_S3	266.0	185	325.4	3.6
	Average (and COV [%])	265.5 (0.20)	183.4 (1.72)	328.0 (1.38)	3.7 (3.34)

Full debonding on the bonded interface around any CHS member will lead to loss of structural integrity (failure) while partial debonding will lead to reduction of secant stiffness of the joint without loss of the structural integrity.

4. Results and discussion

General overview of all test results is given in Table 3 and Table 4. The identification of the failure modes, are presented in the follow-up sections and facilitated by analysis of surface strains obtained by 3D DIC measurements in combination with general load–displacement

Table 4
Test results related to influence of steel grade.

5	A-Ss-R2-PM_S4	245.0	225.7	312.4	6.4
	A-Ss-R2-PM_S5	250.1	224.2	306.8	5.8
	A-Ss-R2-PM_S6	254.7	224.4	311.8	6.1
	Average (and COV [%])	249.9 (1.59)	224.8 (0.30)	310.3 (0.81)	6.1 (4.02)
6	A-Ss-R2-PH_S1	241.8	228.4	571.5	6.3
	A-Ss-R2-PH_S2	241.6	228.1	586.3	5.6
	A-Ss-R2-PH_S3	235.1	226.2	471.8	3.8
	Average (and COV [%])	239.5 (1.30)	227.6 (0.41)	543.2 (9.36)	5.2 (20.12)

curves.

The displacement values in Table 3, 4 and Figs. 7, 8 and 9 are measured based on the two points 50 mm outside the wrapped region on the two steel members, as indicated in Fig. 3.

All specimens of Series 1 to 5 failed by full debonding at the steel-composite interface on one of the steel members preceded by limited or extensive yielding of the steel CHS outside the wrapping area. The debonding initiates and propagates consecutively from the joint root in the middle of the joint towards the wrapping ends. Final debonding failure is due to coalescence of debonding crack from the root and end. The failure process is explained in more details in Section 4.4. In series 6 delamination between the first plies next to the interface is dominant failure mode while yielding of the steel CHS is less evident.

The elastic load limit is governed as initiation of debonding from the root of the bonded interface. For each specimen, the elastic limit is determined as the load level at which the secant stiffness decreases 5%.

4.1. Influence of bonding primer

Fig. 7 shows the load–displacement curves of 6 wrapped composite A-joints of series 1 and 2, without and with application of the bonding primer, respectively. Application of the bonding primer helps improve displacement of the joint at failure by 50% and decrease its scattering by 71%. No significant difference (within 5%) is seen in the initial stiffness and elastic load limit because it depends merely on the elastic properties of composite material and steel.

4.2. Influence of mechanical properties of polymer resins

Fig. 8 shows load–displacement curves of 9 wrapped composite A-joint specimens referring to series 2, 3 and 4 produced with three types of resins R1, R2 and R3, respectively. The joints produced with resin 2 (toughened vinyl ester) show 19%~22% larger elastic load limit and 26%~32% larger displacement at failure, respectively, than the joints produced with resin 1 (regular vinyl ester) and resin 3 (regular polyester).

The fracture toughness of resins has a governing effect on the joints' ultimate displacement (ductility). Larger fracture toughness of resin 2 over the other two resins contributes to less rapid debonding crack propagation in the joint and resulting in larger displacement at failure, thus improved ductility of the joint.

4.3. Influence of CHS steel grade

Fig. 9 depicts the load–displacement behavior of 3 mild steel (MS) and 3 high-strength steel (HSS) wrapped composite A-joint specimens. 75% larger ultimate joint load is observed in HSS joint specimens. The initial stiffness is the same as in case of MS joint specimens. While full

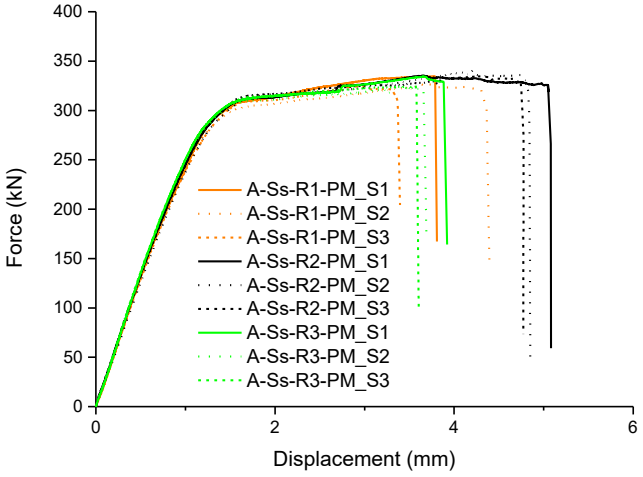

Fig. 8. Tensile static behavior of wrapped composite A-joints produced with three types of resins.

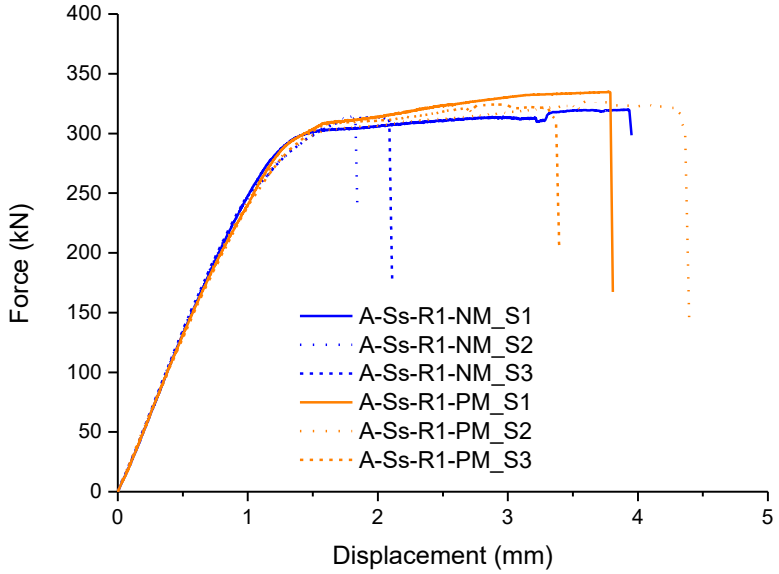

Fig. 7. Tensile static behavior of wrapped composite A-joint applied with vs without bonding primer.

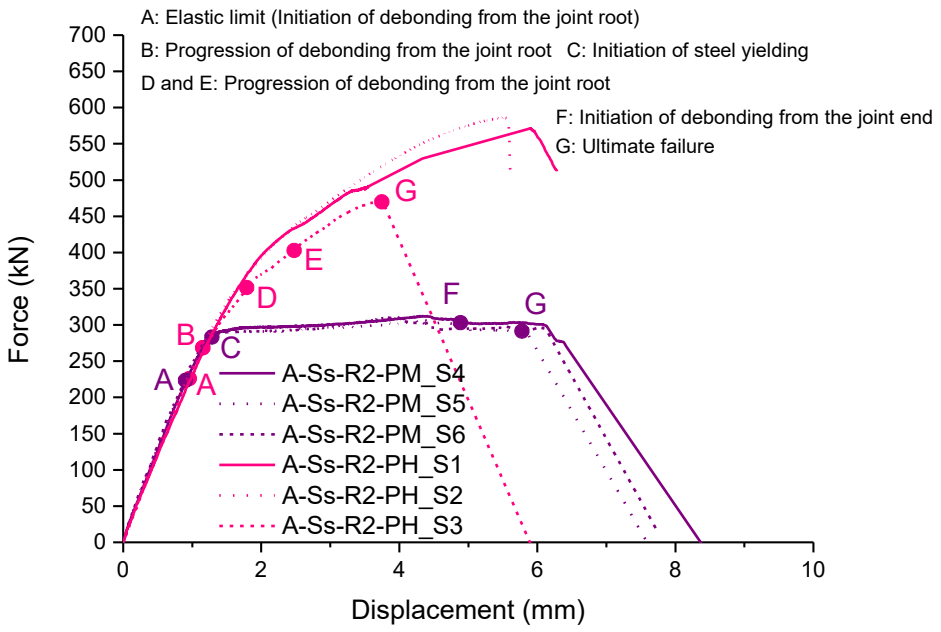

Fig. 9. Tensile static behavior of MS vs. HSS wrapped composite joints.

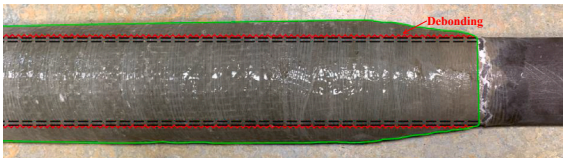

a) MS joints fails at the steel-composite bonded interface (full debonding)

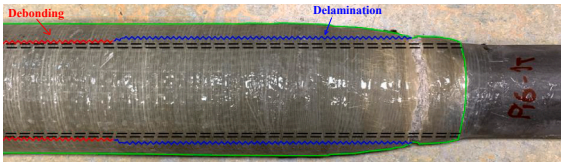

b) HSS joints failing due to combined debonding and delamination

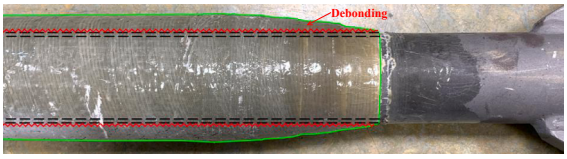

c) HSS joint with lowest resistance failing due to full debonding

Fig. 10. Comparison of the failure modes between MS and HSS A-joints.

debonding on the bonded interface is the governing failure mode of all MS joints, two out of three HSS joints (A-Ss-R2-PH_S1 and S2) fail due to combined debonding and delamination. Still, one of the HSS specimens A-Ss-R2-PH_S3 fails in the same manner as MS specimens, by full debonding, as shown in Fig. 10. This specimen had lowest resistance in the HSS series experiments.

One of the HSS joints with combined debonding-delamination failure (A-Ss-R2-PH_S1) is cut through its mid-plane after the experiments to investigate the failure process, as shown in Fig. 11. The cut surface is grinded by sand paper and polished. The failure is initiated by debonding on the interface at the wrap root (junction of steel tubes) which propagates to a certain length (region a-b in Fig. 11). At approximately 100 mm of the debonding length the crack transfers into the inter-laminar interface between the first and the second ply of the

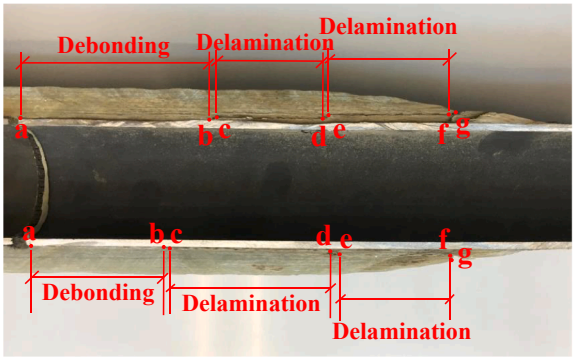

Fig. 11. Crack path in cut HSS specimen (A-Ss-R2-PH_S1).

composite wrap (region c-d). The delamination transfers further into the interface between the 2nd and 3rd ply (e-f), and the final failure is reached by growth of the delamination towards the composite wrap end (point g).

4.4. Crack propagation in mild steel vs. high-strength steel A-joint specimens

In the experimental results presented so far for the MS joint specimens, full debonding of the bonded interface is reached after yielding of steel tube. Steel yielding leads to contraction of the steel cross-section outside the wrapped region, resulting in Mode I (peel stress dominated) debonding crack initiation and propagation from the wrap end and finally coalescence with the debonding crack propagated from the wrap root. Therefore, resistance of the bonded interface is limited by yielding of steel. In wrapped composite joints with HSS, yielding and excessive contraction of the steel cross-section outside the composite wrap is excluded. Therefore, debonding at the wrap end is prevented which is the main reason why much larger debonding resistance is reached despite that the dimensions of the composite wrap and the surface preparation are the same as in case of MS joint specimens.

In order to substantiate the explained difference in failure behavior, ultrasonic scanning was attempted including phased array alternative to measure the debonding length but unfortunately no useful and

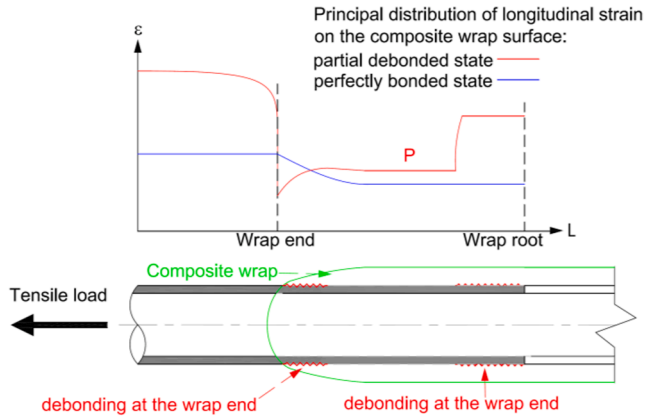

Fig. 12. Principle of using variation of the distribution of longitudinal surface strains on composite wrap to determine debonding crack length in the embedded bonded interface.

conclusive results was obtained. The main reasons for unsuccessful measurements are the relatively large thickness (14 mm) curved surface and unclear reflection from steel to composite interface. The analysis of development of debonding cracks in MS and HSS specimens is then performed with help of DIC results. Fig. 12 gives the explanation of physical analogy that is used to determine the debonding crack length by using longitudinal surface strains obtained from DIC in experiments. In the perfectly bonded state, steel and composite in an arbitrary cross section are connected and carry the external force in a manner of hybrid (composite) circular cross section. The longitudinal strains along the steel tube and the composite wrap are of similar magnitude, as indicated by the blue line. Strains are slightly diminished in the region of the composite wrap due to larger cross section (steel + composite) resisting the external load. Still the distribution of longitudinal surface strain along the longitudinal path is relatively uniform and monotonic. In the partially debonded state, by contrast, a deviation of such monotonic state would exist. In case of debonding at the wrap root an increase of surface strain will occur because in that region the external force is no longer resisted by a hybrid steel + composite cross section but by the composite part of the cross-section only. In similar fashion the surface strains in the region of debonding at the wrap end would be decreased compared to the bonded area. This is because the composite part of the cross section which is on the outside is debonded and no longer transfers the external load.

Development of surface strains (longitudinal strains) of 2 specimens, A-Ss-R2-PM_S5 and A-Ss-R2-PH_S3, are shown in Figs. 13 and 15, respectively, to characterize the failure process of MS and HSS wrapped composite A-joints. Critical load stages are identified in the load–displacement curves in Fig. 9 to explain the two different failure process related to debonding with or without yielding of the steel members. Wrapped composite joints behave elastic in both cases as shown in Fig. 13a) and 15a) until approximately 225 kN (point A). The end of linear elastic behavior is attributed to initiation of debonding from the joint root between the composite wrap and the steel member due to shear stress on the interface, see Fig. 13 b) and 15b). As for the MS joint, debonding crack propagates steadily from the joint root followed by initiation of steel yielding at the wrap end at 289kN (point C), see Fig. 13c). Additional debonding crack is initiated from the joint end at 306 kN (point F) when the bonded interface at the wrap end cannot resist the peel stress due to contraction of the steel cross section after yielding (see Fig. 13d)). Debonding crack then develops significantly to the critical length at 291 kN (point G) and its coalescence with the debonding crack from the wrap root leads to full debonding, as shown in Fig. 13e). By contrast, debonding crack from the root of the HSS joint consistently propagates (point B, D and E, see Fig. 15 c), d) and e)) without steel yielding until reaching the critical length at 464 kN (point

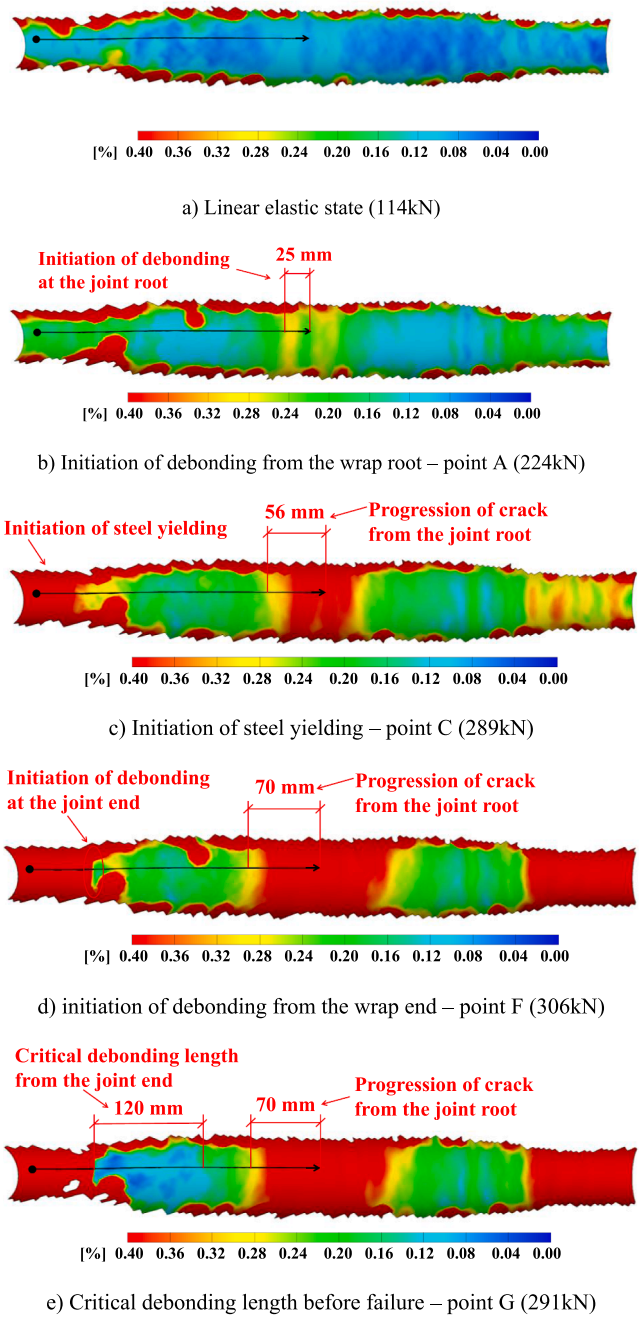

Fig. 13. Longitudinal surface strains of a mild-steel specimen (A-Ss-R2-PM_S5) at critical loading stages indicating failure process.

G, see Fig. 15 f)) and leads to full debonding of the bonded interface.

Crack lengths at the characteristic load stages are analyzed along a path which is defined in longitudinal direction, starting at the free end of the composite wrap and ending at the root connection, as indicated in Fig. 13 and Fig. 15. The longitudinal surface strains along the path obtained at characteristic loading stages of the MS and HSS joint are shown in Fig. 14 a) and Fig. 16 a), respectively. The aim is to identify indirectly the debonding crack length by observing local increase or decrease of surface strains at the crack front. To this aim the surface strains at all stages are normalized to strains that would correspond to the elastic load stage in Fig. 14 b) and Fig. 16 b) for MS and HSS, respectively. If there would be no debonding, delamination, composite cracking and/or steel yielding, the normalized strains at later load stages would be identical to the reference elastic state. The deviations from such idealistic state are

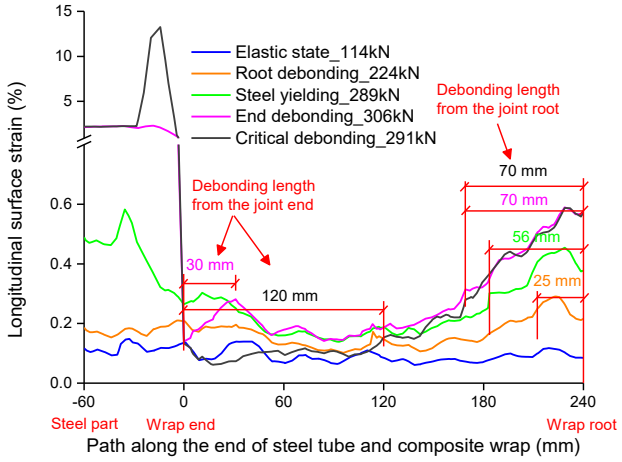

a) Strains at characteristic loading states corresponding to progression of failure

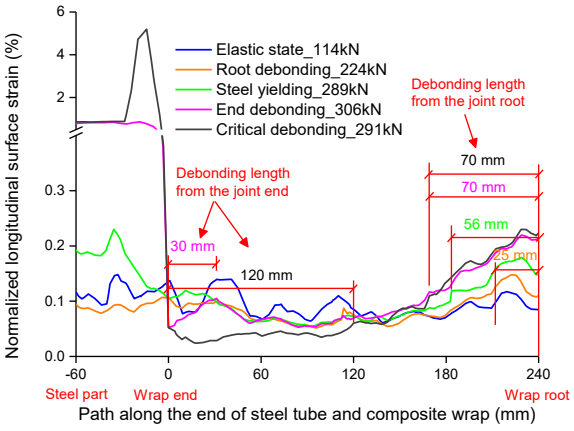

b) Strains normalized to load level corresponding to the elastic state (114 kN)

Fig. 14. Longitudinal surface strains along the end of steel tube and composite wrap of a mild-steel specimen (example of A-Ss-R2-PM_S5).

used to identify fronts of the debonding cracks that are observed after cutting of the specimens. The threshold of the strain level to quantify debonding crack length varies from 0.15% to 0.3% while it becomes more or less constant and is approximately 0.1% after strain normalizing. These values are chosen on judgment of location of the strains front at which the strain would significantly increase from flat line to higher strain region. This method is verified in the investigation where FE model are used to determine the threshold [19].

Surface strains distribute uniformly without steep increase along the path in the linear elastic stage, the load level of 114 kN before point A indicated in Fig. 9. Significant steep increase of surface strain from 0.1% to 0.3% indicates that debonding is initiated from the wrap root with 25 mm debonding length at load level 225kN (point A). In the MS joint, debonding length at the root steadily increases to 56 mm at 289 kN corresponding to initiation of steel yielding – point C in Fig. 9, and consistently grows to 70 mm at 306 kN where debonding is initiated from the wrap end – point F in Fig. 9. Debonding crack from the wrap root subsequently stops increasing because all energy is dissipated in propagation of debonding crack from the wrap end. The critical length of the debonding crack of 190 mm (79% of full bonding length) is recorded just before ultimate failure (see Fig. 14) when the coalescence of the crack initiated at the wrap root and wrap end is reached due to

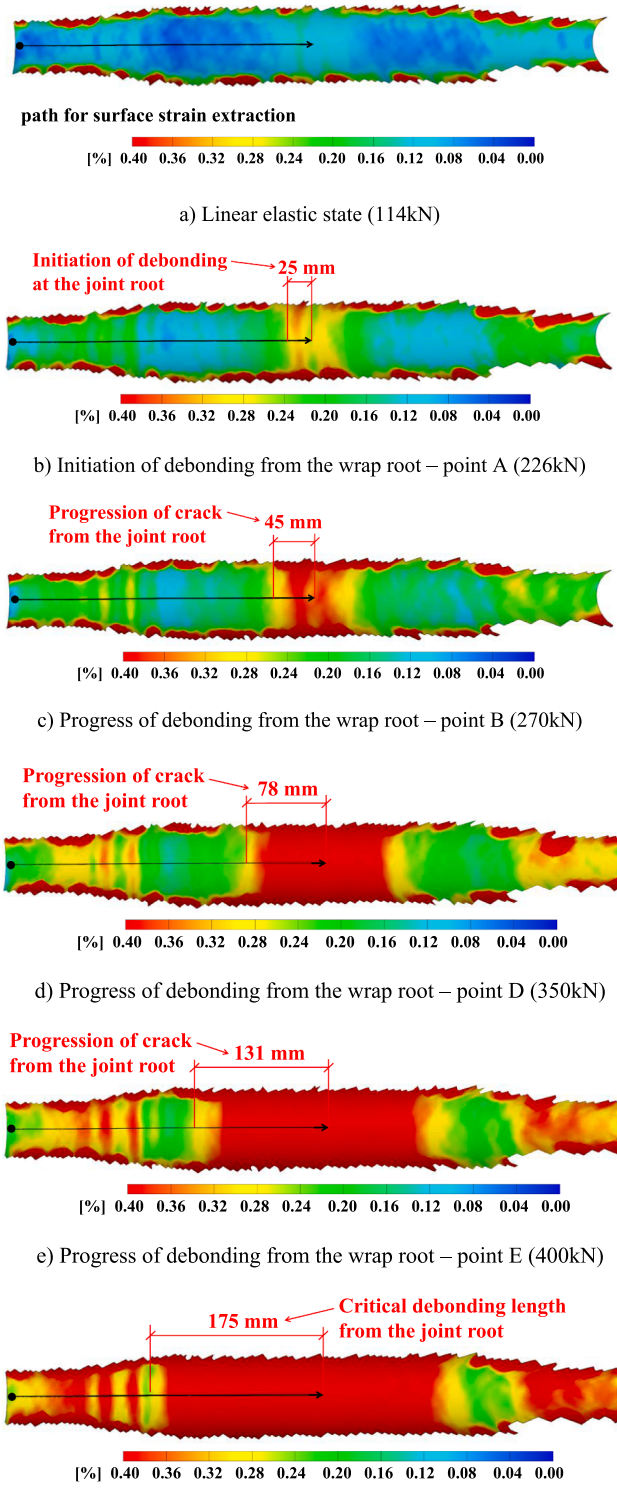

a) Linear elastic state (114kN)

b) Initiation of debonding from the wrap root – point A (226kN)

c) Progress of debonding from the wrap root – point B (270kN)

d) Progress of debonding from the wrap root – point D (350kN)

e) Progress of debonding from the wrap root – point E (400kN)

f) Critical debonding length before failure – point G (464kN)

Fig. 15. Longitudinal surface strains of a high-strength steel specimen (A-Ss-R2-PH_S3) at critical loading states indicating failure process.

excessive yielding of steel outside the wrap with approximately 2.2% of plastic strain (see Fig. 14 a)). Conversely, debonding crack from the root of the HSS joint steadily increases to 45 mm, 78 mm and 131 mm at 270 kN, 350 kN and 400 kN (point B, D and E in Fig. 9), respectively, without steel yielding and without debonding initiated from the wrap end. The debonding crack subsequently propagates to the critical length of 175

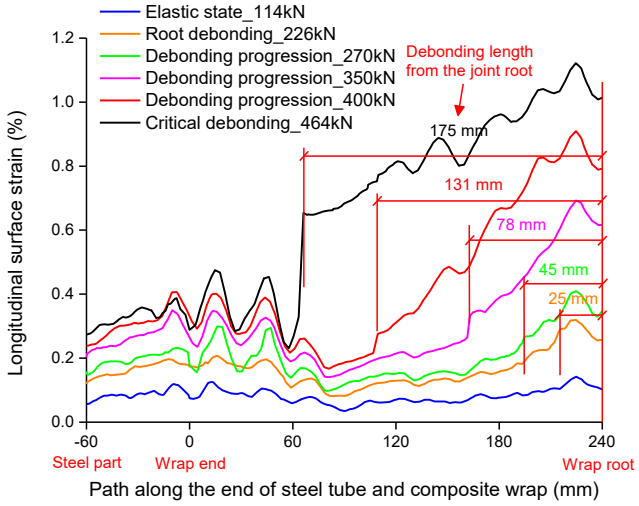

a) Strains at characteristic loading states corresponding to progression of failure

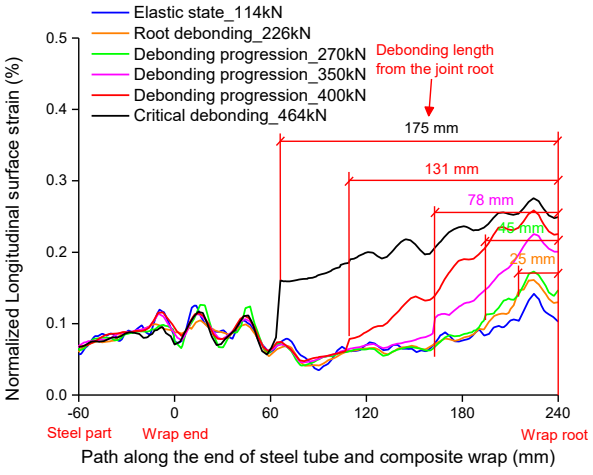

b) Strains normalized to load level corresponding to the elastic state (114 kN)

Fig. 16. Longitudinal surface strains along the end of steel tube and composite wrap of a high-strain steel specimen (example of A-Ss-R2-PH_S3).

mm (73% of full bonding length) just before ultimate failure (see Fig. 16). At the wrap end, strain localization is observed due to ply drops during the loading process as presented in Fig. 16.

Development of debonding in MS and HSS joints is compared in Fig. 18 with respect to the applied load level. The propagation rate of the crack propagating from the wrap root is almost identical for MS and HSS joint until the load level at which steel yielding in MS joint initiates the debonding from the wrap end. Propagation of debonding at the wrap end in MS joints is exhibited at non-increasing load level, however with the increasing joint displacement, as shown in load–displacement graphs in Fig. 9. This behavior is attributed to steel CHS yielding as indicated in Fig. 17 a) by contraction (necking) of the steel cross section of MS joints outside the composite wrap. It is shown in Section 4.2 that more ductile resin would contribute in retarding the propagation of the debonding crack at the wrap end. Development of the debonding crack in the wrap root in the HSS joint is steady until final failure. The debonding from the wrap end is excluded because of absence of steel yielding (necking) in the CHS outside the composite wrap, see Fig. 17 b).

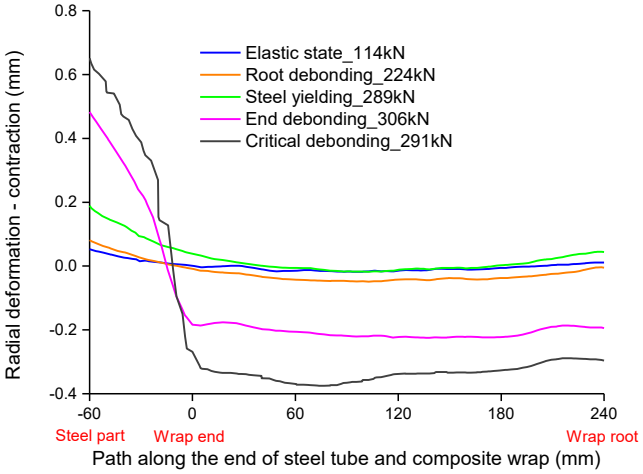

a) Mild-steel specimen

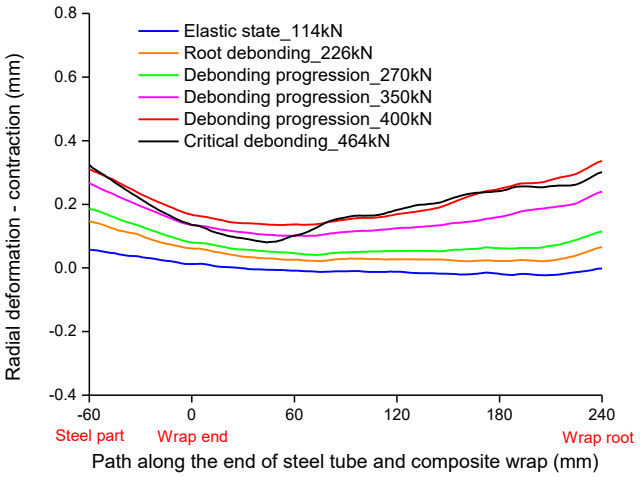

b) High-strength steel specimen

Fig. 17. Radial deformation of the steel tubes outside the composite wrap indicating the necking behavior.

5. Conclusions

Six series of ultimate load experiments were conducted to identify the influence of production parameters (i.e., with and without bonding primer; 3 types of polymer resin types; steel grade S355 and S700) on the static behavior of wrapped composite joints connecting steel members solely through bonding as the alternative to welded CHS joints. Uniaxial (splice) joint loaded in axial tension (A-joint) geometry was chosen for clear interpretation of the mechanical behavior and identification of the debonding in the ultimate load experiments. A novel method of identifying debonding crack length by help of surface strains obtained by 3D DIC is explained and employed to analyze failure behavior of the joint specimens. Following conclusions are drawn:

1) Full debonding on the bonded interface preceded by steel yielding outside the composite wrap is the ultimate failure mode of the wrapped composite joints with mild-steel. Failure of joints with high strength steel is due to combined debonding at the wrap root and delamination towards the wrap end.

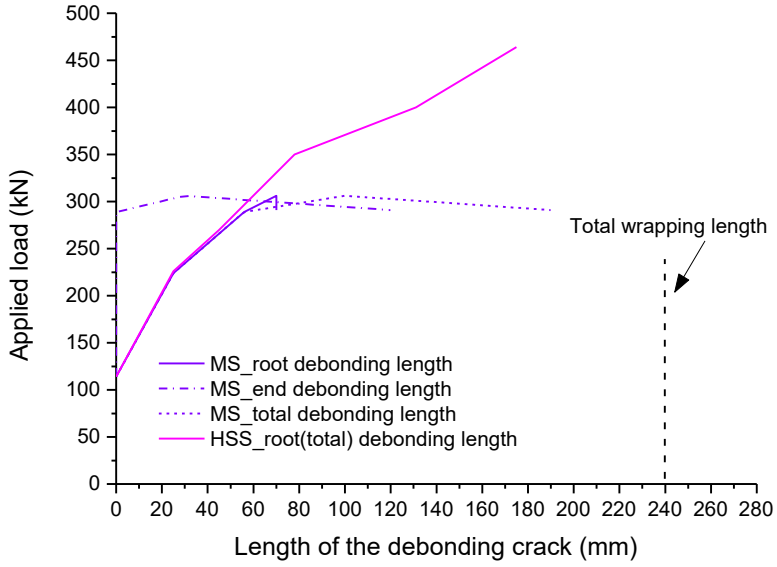

Fig. 18. Comparison of crack length growth in MS and HSS specimens.

2) Interaction between debonding and steel yielding is limiting utilization of the resistance of the bonded interface in the mild-steel joints. Main reason is initiation and propagation of the debonding crack due to yielding contraction (necking) of the steel-cross section at the wrap end. Wrapped composite joints with high strength steel exhibits 75% larger ultimate joint load where steel yielding is prevented.
3) The fracture toughness of polymer resins has a governing effect on the ductility of wrapped composite joints. Larger fracture toughness of the resin helps delay the initiation of debonding crack in mode I from the wrap end due to the steel cross-section contraction.
4) Larger fracture toughness of a toughened vinyl-ester resin over a regular vinyl-ester resin and a polyester resin contributes to 20% larger elastic load limit and 30% larger failure displacement of wrapped composite A-joints, respectively.
5) Application of the bonding primer to improves chemical bonding properties results in improved ductility by approx. 50% larger displacement of the joint at failure and decreases its scattering in respect of displacement at failure.

In the future the results in terms of finite element analysis of wrapped composite joints will be presented to replicate and explicitly explain the debonding process, and investigated the size effect on the joint resistance.

CRediT authorship contribution statement

Pei He: Investigation, Data curation, Writing – original draft, Visualization. **Weikang Feng:** Investigation, Data curation, Visualization. **Marko Pavlovic:** Conceptualization, Methodology, Supervision, Project administration, Funding acquisition.

Declaration of Competing Interest

The authors declare that they have no known competing financial interests or personal relationships that could have appeared to influence the work reported in this paper.

Data availability

The data that has been used is confidential.

Acknowledgments

This research is supported by NWO (Netherlands Organization for Scientific Research) under Demonstrator project "Fatigue resistant Wrapped FRP joints of structural hollow sections", proj. no. 16949. The first author would also like to express his gratitude for the financial support from China Scholarship Council (CSC) under grant number of 201806260242. The authors are grateful for the acknowledge provision and fabrication of the wrapped composite joints by Tree Composites b. v., Versteden b.v.and Ask Romein b.v. The authors are very grateful for the assistance of technicians from Steven Lab II of TU Delft.

Data availability statement.

The raw/processed data required to reproduce these findings cannot be shared at this time as the data also forms part of an ongoing study.

References

[1] Wardenier J, Packer JA, Zhao XL, Van der Vegte GJ. Hollow sections in structural applications. Rotterdam, The Netherlands: Bouwen met staal; 2002.
[2] Vuong N, Quan M. Fatigue analysis of jacket support structure for offshore wind turbines. J Sci Technol Civil Eng (STCE) - HUCE. 2019;13, 1 (Jan. 2019), 46–59.
[3] Siriwardane SC, Adasooriya ND, Pavlou D. Fatigue Strength Curve for Tubular Joints of Offshore Structures under Dynamic Loading. Dynamics 2021;1(1): 125–33.
[4] Naser Shabakhty & Seyed Saeid Tabatabaei. Sensitivity of fatigue assessment for offshore jacket platform to different pile–soil–structure interaction models. Ships Offshore Struct 2021. https://doi.org/10.1080/17445302.2021.1979919.
[5] Nussbaumer A, Borges L, Davaine L. Fatigue design of steel and composite structures: Eurocode 3: Design of steel structures, part 1-9 fatigue; Eurocode 4: Design of composite steel and concrete structures. John Wiley & Sons; 2012.
[6] Jiao H, Zhao XL. CFRP strengthened butt-welded very high strength (VHS) circular steel tubes. Thin-Walled Struct 2004;42(7):963–78.
[7] Haedir J, Bambach MR, Zhao XL, Grzebieta RH. Strength of circular hollow sections (CHS) tubular beams externally reinforced by carbon FRP sheets in pure bending. Thin-Walled Struct 2009;47(10):1136–47.
[8] Lesani M, Bahaari MR, Shokrieh MM. Numerical investigation of FRP-strengthened tubular T-joints under axial compressive loads. Compos Struct 2013;100:71–8.
[9] Lesani M, Bahaari MR, Shokrieh MM. Experimental investigation of FRP-strengthened tubular T-joints under axial compressive loads. Constr Build Mater 2014;53:243–52.
[10] Lesani M, Bahaari MR, Shokrieh MM. FRP wrapping for the rehabilitation of Circular Hollow Section (CHS) tubular steel connections. Thin-Walled Struct 2015; 90:216–34.
[11] Fu Y, Tong L. Experimental Study on Behavior of CFRP-Strengthened Circular Hollow Section Gap K-Joints, 6th International Conference on Advances in Experimental Structural Engineering, University of Illinois, Urbana-Champaign, United States, August 1-2; 2015.
[12] Fu Y, Tong L, He L, Zhao XL. Experimental and numerical investigation on behavior of CFRP-strengthened circular hollow section gap K-joints. Thin-Walled Struct 2016;102:80–97.

[13] Pavlovic M, Veljkovic M, Bogers P. Method for making a virgin joint between two separate structural hollow sections, and such a virgin joint.
[14] Liatzouras M. Feasibility of non-welded CHS steel joints adhesively bonded by GFRP, MSc thesis, Delft University of Technology, Delft; 2018.
[15] Pavlovic M, Veljkovic M, Liatzouras M. Wrapped FRP Joints of Steel Hollow Sections, Eighth International Conference on THIN-WALLED STRUCTURES – ICTWS 2018, Lisbon, Portugal, July 24-27; 2018.
[16] He P, Pavlovic M. Feasibility of Wrapped FRP Circular Hollow Sections Joints, Proceedings of the 17th International Symposium on Tubular Structures, National University of Singapore, Singapore, December 9-12; 2019.
[17] Feng W, Pavlovic M. Fatigue behaviour of non-welded wrapped composite joints for steel hollow sections in axial load experiments. Eng Struct 2021;249:113369.
[18] He P, Pavlovic M. Failure modes of bonded wrapped composite joints for steel circular hollow sections in ultimate load experiments. Eng Struct 2022;254:113799.
[19] Feng W, Pavlovic M. Combined DIC and FEA method for analysing debonding crack propagation in fatigue experiments on Wrapped Composite Joints, Composite Structures, Accepted with minor revision.
[20] Kwakernaak A, Hofstede J, Poulis J, Benedictus R. Improvements in bonding metals for aerospace and other applications. In: Welding and Joining of Aerospace Materials (pp. 229-275). Woodhead Publishing; 2012.
[21] Adams, R.D. ed., 2021. Adhesive bonding: science, technology and applications. Woodhead Publishing.
[22] Shahid M, Hashim SA. Effect of surface roughness on the strength of cleavage joints. Int J Adhes Adhes 2002;22(3):235–44.
[23] Şekercíoğlu T, Rende H, Gülsöz A, Meran C. The effects of surface roughness on the strength of adhesively bonded cylindrical components. J Mater Process Technol. 2003;142(1):82–86.
[24] Uehara K, Sakurai M. Bonding strength of adhesives and surface roughness of joined parts. J Mater Process Technol 2002;127(2):178–81.
[25] Azari S, Papini M, Spelt JK. Effect of surface roughness on the performance of adhesive joints under static and cyclic loading. J Adhes 2010;86(7):742–64.
[26] Ebnesajjad S, Landrock AH. Adhesives technology handbook. William Andrew; 2014.
[27] Kinloch AJ, Kinloch AJ. Adhesion and adhesives: science and technology. Springer Science & Business Media; 1987.
[28] Snogren RC. Handbook of surface preparation. New York, NY: Palmerton Publishing Co.; 1974. ISBN: 0686482212.
[29] Akers SC. The function of adhesive primers in adhesive bonding of aircraft structures. In: Bodnar MJ, editor. Applied polymer symposia no. 19, processing for adhesives bonded structures. New York, NY: Interscience Publisher; 1972. pp. 23-8.
[30] DeLollis, Nicholas J. Adhesives, adherends, adhesion. 1980.
[31] Da Silva LF, Rodrigues TNSS, Figueiredo MAV, De Moura MFSF, Chousal JAG. Effect of adhesive type and thickness on the lap shear strength. J Adhes 2006;82(11):1091–115.
[32] Liao L, Huang C, Sawa T. Effect of adhesive thickness, adhesive type and scarf angle on the mechanical properties of scarf adhesive joints. Int J Solids Struct 2013;50(25–26):4333–40.
[33] Liao L, Huang C. Numerical analysis of effects of adhesive type and geometry on mixed-mode failure of adhesive joint. Int J Adhes Adhes 2016;68:389–96.
[34] International Standard Organization. ISO 527-1:2019, Plastics — Determination of tensile properties — Part 1: General principles.
[35] International Standard Organization. ISO 527-2: 2012, Plastics — Determination of tensile properties — Part 2: Test conditions for moulding and extrusion plastics.
[36] International Standard Organization. ISO 14126:1999, Fibre-reinforced plastic composites — Determination of compressive properties in the in-plane direction.
[37] International Standard Organization. ISO 14129:1997, Fibre-reinforced plastic composites — Determination of the in-plane shear stress/shear strain response, including the in-plane shear modulus and strength, by the plus or minus 45 degree tension test method.